I&EC research
Industrial & Engineering Chemistry Research

Article

Cite This: Ind. Eng. Chem. Res. 2019, 58, 14719−14728

pubs.acs.org/IECR

Post Plasma Catalysis for the Removal of Acetaldehyde Using Mn−Co/HZSM-5 Catalysts

Tian Chang,[†,‡,§] Jiaqi Lu,[†] Zhenxing Shen,*[,†,§] Bin Zhang,[†] Yu Huang,[§] Junji Cao,[§] Hongxia Liu,[†] Savita K. P. Veerapandian,[‡] Nathalie De Geyter,[‡] and Rino Morent[‡]

[†]Department of Environmental Sciences and Engineering, Xi'an Jiaotong University, Xi'an 710049, China

[‡]Research Unit Plasma Technology, Department of Applied Physics, Faculty of Engineering and Architecture, Ghent University, Sint-Pietersnieuwstraat 41-B4, 9000 Ghent, Belgium

[§]Key Lab of Aerosol Chemistry & Physics, SKLLQG, Institute of Earth Environment, Chinese Academy of Sciences, Xi'an 710049, China

Supporting Information

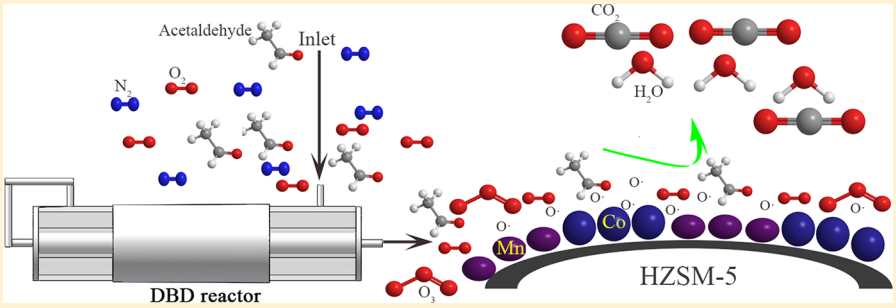

ABSTRACT: A system combining nonthermal plasma (NTP) and catalysis using Mn−Co/HZSM-5 catalyst has been developed to promote the oxidation of acetaldehyde and reduce the production of ozone. The introduction of catalyst improved the oxidation of acetaldehyde and inhibited the generation of O_3 in comparison with the NTP alone system. The mixed MnCo/HZSM-5 catalyst demonstrated the highest catalytic activity among the various prepared catalysts, and this was ascribed to its crystalline structure, redox property, and adsorbed surface oxygen of the catalyst. The removal efficiency of acetaldehyde and CO_x yield were positively associated with the specific energy density (SED), and they were inversely related to the gas flow rate. Nevertheless, the energy yield was in negative correlation with the SED and in positive association with the gas flow rate. Moreover, the impact of different catalysts on the acceleration of acetaldehyde degradation in the hybrid system was discussed by developing a simple kinetic model.

1. INTRODUCTION

Volatile organic compounds (VOCs) which are released from multiple transportation vehicles and industries form a dominant source of air pollution.[1] Due to their malodorous, toxic, mutagenic, and carcinogenic nature, the removal of VOCs has gained public concern.[2] VOCs are also associated with the formation of photochemical smog as they are the precursors of smog and ozone.[1] Due to the hazardous effect of VOCs on human health and the environment, the investigations to remove these harmful VOCs from the environment have been accelerated.[3,4] Conventional technologies include absorption, catalytic oxidation, membrane separation, and biological treatment, which are not economical for the elimination of dilute VOCs from a large volume of gas.[2] Recently, nonthermal plasma (NTP) has drawn interest in VOCs abatement due to its high reactivity at mild conditions.[5] However, the low product selectivity and the generation of undesired and toxic byproducts limit the industrial application of NTP technology.[1,2] It has been already demonstrated that the product selectivity of NTP technology can be improved by combining it with catalysis. The heterogeneous catalyst could be put inside or after the plasma discharge region.[6] For the former, the catalyst could utilize the short-lived species formed in the discharge process and enhance the electric field intensity.[7] However, for the latter, the catalyst could utilize the ozone and remove byproducts generated in the discharge region.[7] In addition, numerous parameters such as gas flow rate, discharge power, and water can influence the reaction performance of the NTP-catalytic system via changing the reaction time and chemical species formed in the discharge process and catalytic reaction process.[8,9]

Catalysts occupy a vital position in the NTP-catalytic system by effectively utilizing the reactive oxygen species produced in the discharge zone, thus leading to a synergetic effect between NTP and catalyst.[6] So far, numerous works have been carried

Received: May 15, 2019
Revised: July 15, 2019
Accepted: July 19, 2019
Published: July 31, 2019

DOI: 10.1021/acs.iecr.9b02668
Ind. Eng. Chem. Res. 2019, 58, 14719−14728

out for the investigation of the metal-based catalysts in NTP-catalytic systems.[3,10] Among the various metal-based catalysts, transition metal catalysts are superior to supported noble metal catalysts owing to their low cost. In particular, manganese and cobalt-based catalysts have been extensively investigated based on their remarkable potential applications in decomposing ozone at room temperature.[11] For Mn-based catalysts, the high catalytic activity is attributed to their multiple oxidation states and high activity and Co-based catalysts are reported to show efficient total oxidation of VOCs.[12] Also, the mixed oxide catalysts possess better catalytic activity than the single oxide catalysts due to the synergistic effect between different metal oxides. Besides the loaded metals/metal oxides, the catalyst supports also occupy a major role in the effectiveness of the catalysts.[13] HZSM-5 zeolite has been widely used for VOCs elimination due to its relatively high adsorption ability, special mesoporous structure, and high hydrothermal stability.[14] Thus, Mn and Co oxides loaded on the HZSM-5 may enhance the catalytic properties of the composite materials. However, up until now, very few works have been done on a thorough and systematic study of VOCs degradation over mixed oxides loaded on the HZSM-5, especially in the post NTP-catalytic (PPC) process.[10,15]

In this work, acetaldehyde was used as a model VOCs due to its wide usage and its hazardous effect on human health and the environment. A PPC system combining a DBD reactor and various Mn−Co/HZSM-5 catalysts were used to study the acetaldehyde decomposition. The effect of different Mn−Co/HZSM-5 catalysts and various experimental parameters such as gas flow rate and SED on the removal efficiency of acetaldehyde, CO_2 yield, CO_x yield, and energy yield (EY) were investigated. To obtain deeper insight into the influence of the catalyst properties on acetaldehyde removal, multiple characterization techniques like X-ray diffraction (XRD), high-resolution-transmission electron microscopy (HR-TEM), and hydrogen-temperature-programmed reduction (H_2-TPR) were performed. In addition, the reaction kinetics for the degradation of acetaldehyde in the PPC system over different catalysts were discussed using a steady-state approximation method based on the experimental results.

2. EXPERIMENTAL SECTION

2.1. Catalyst Synthesis and Characterization. A deposition-precipitation method was used to synthesize the Mn−Co/HZSM-5 (the molar ratio of Mn/Co = 1) catalysts. $Mn(NO_3)_2{\cdot}4H_2O$ and $Co(NO_3)_3{\cdot}9H_2O$ were selected as the precursors, meanwhile, the HZSM-5 zeolite was used as the support. In a typical synthesis, in the first step aqueous solutions of $Co(NO_3)_2$ (0.5 mol L^{-1}) and $Mn(NO_3)_2$ (0.6 mol L^{-1}) were mixed by continuous magnetic stirring. Subsequently, HZSM-5 zeolite was added to the solution under stirring. Then, $KMnO_4$ (0.4 mol L^{-1}) was introduced into the acquired slurry and stirred at 60 °C for 1 h. After that, the pH of the above mixture was tuned to 9 by dropwise addition of Na_2CO_3 and the stirring at 60 °C was continued for 4 h. Lastly, the sample was obtained by filtration, drying, and calcination at 500 °C for 3 h. Also, MnO_x and Co_3O_4 loaded on the HZSM-5 were synthesized using the above-mentioned method. The samples were expressed as Mn/HZ-5, Co/HZ-5, and MnCo/HZ-5.

The characterizations of the catalyst samples were analyzed by XRD, Raman, the N_2 adsorption−desorption isotherms, inductively coupled plasma emission spectrometry (ICPES), scanning electron microscopy (SEM), HR-TEM, XPS, and H_2-TPR as described in our previous studies.[16,17] The ammonia-temperature programmed desorption (NH_3-TPD) was operated to study the surface acidity of the catalyst. The NH_3-TPD analysis started with the pretreatment of 200 mg of catalyst in argon at 300 °C for 1 h. Then, the adsorption of NH_3 (10%, Ar as balance gas) was conducted at 30 °C until saturation which took about 1.5 h. Subsequently, the excess NH_3 was wiped away by flushing the sample with pure argon. Finally, the NH_3 desorption was operated by heating the sample to 800 °C.

2.2. Experimental Setup. As displayed in Figure 1, the overall setup included a gas supply system, PPC system, and

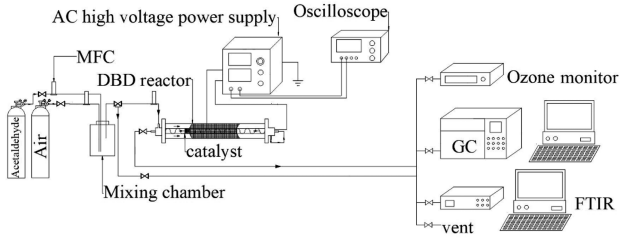

Figure 1. Diagram of the experimental setup.

analysis system. The detailed description of the DBD reactor, oscilloscope, ac high-voltage power supply, as well as the calculation of the discharge power were reported in our previous work.[16,17]

2.3. Post NTP Catalysis. The post NTP catalysis for acetaldehyde removal was conducted at ambient pressure and temperature using dry air with a fixed volume ratio of O_2/N_2 (1/4) as carrier gas. The desired initial concentration of acetaldehyde was obtained by tuning the ratio of purge of acetaldehyde and carrier gas. The gas flow rate was tuned by a mass flow controller (MFC, Sevenstar D07-series, China). The initial concentration of acetaldehyde was set as 200 ppm. The range of the total gas flow rate was 0.5−1.5 L min^{-1}. Catalyst (0.2 g) was put in the downstream of the NTP discharge zone by quartz-wool loading. It was purified at 300 °C for 3 h in the N_2 flow before use. The concentration of acetaldehyde was measured continuously using an online Fourier transform infrared spectroscopy (Gasmet DX4015, Finland) with a fixed resolution of 8 cm^{-1}. The concentration of CO_2 and CO were determined by gas chromatography (GC 9790 II, Fuli, China). A UV-based ozone (O_3) analyzer (2B, 106M) was used to analyze the concentration of O_3. All the reported experimental data in this work are an average of results obtained in three repeated experiments.

The acetaldehyde removal efficiency ($\eta_{acetaldehyde}$), SED, EY, CO_2 yield, and CO_x yield were defined as follows:

$$\eta_{acetaldehyde}(\%) = \frac{[acetaldehyde]_{inlet} - [acetaldehyde]_{outlet}}{[acetaldehyde]_{inlet}} \times 100\% \quad (1)$$

$$SED\ (J\ L^{-1}) = \frac{discharge\ power\ (W)}{gas\ flow\ rate\ (L\ min^{-1})} \times 60\ (s\ min^{-1}) \quad (2)$$

$$EY\ (g\ kWh^{-1}) = \frac{M_{acetaldehyde} \times \eta_{acetaldehyde}}{SED} \times \frac{3.6}{V_m} \quad (3)$$

DOI: 10.1021/acs.iecr.9b02668
Ind. Eng. Chem. Res. 2019, 58, 14719−14728

$$CO_2 \text{ yield } (\%) = \frac{[CO_2]}{2 \times ([\text{acetaldehyde}]_{\text{inlet}} - [\text{acetaldehyde}]_{\text{outlet}})} \times 100\% \quad (4)$$

$$CO_x \text{ yield } (\%) = \frac{[CO] + [CO_2]}{2 \times ([\text{acetaldehyde}]_{\text{inlet}} - [\text{acetaldehyde}]_{\text{outlet}})} \times 100\% \quad (5)$$

where $M_{\text{acetaldehyde}}$ and V_m represents the molar mass of acetaldehyde (g mol^{-1}) and molar volume (L mol^{-1}).

3. RESULTS AND DISCUSSION

3.1. Characterizations of Catalysts. *3.1.1. Crystal Structure and Surface Characteristics.* XRD was carried out to determine the crystalline structure of the fresh catalysts. As displayed in Figure 2a, all the XRD patterns showed a series of peaks which are characteristics of HZSM-5,[18] revealing that the crystalline texture of HZSM-5 remained after Mn and Co loading. However, with Mn and Co loading, the peak intensity of the characteristics peaks of HZSM-5 weakened, while no obvious new peak appeared. This phenomenon is in reasonable agreement with the literature,[13,19] which reveals a good dispersion of manganese and cobalt oxides on the HZSM-5 surface. The intensity of XRD peaks of MnCo/HZ-5 was lower and wider compared with those of Mn/HZ-5 and Co/HZ-5, indicating the possible interaction between Mn and Co species on the catalysts, which improves the dispersion and inhibits the crystallization. This also indicated that the bimetal oxides possess a relative smaller crystalline size in comparison with the monomer oxides. As expected, the particle size (Table 1, calculated using the Scherrer equation[20]) of MnCo/HZ-5 was lower than Mn/HZ-5 and Co/HZ-5. The smaller particle size of the catalyst provides more active sites which accelerate the chemical reactions.

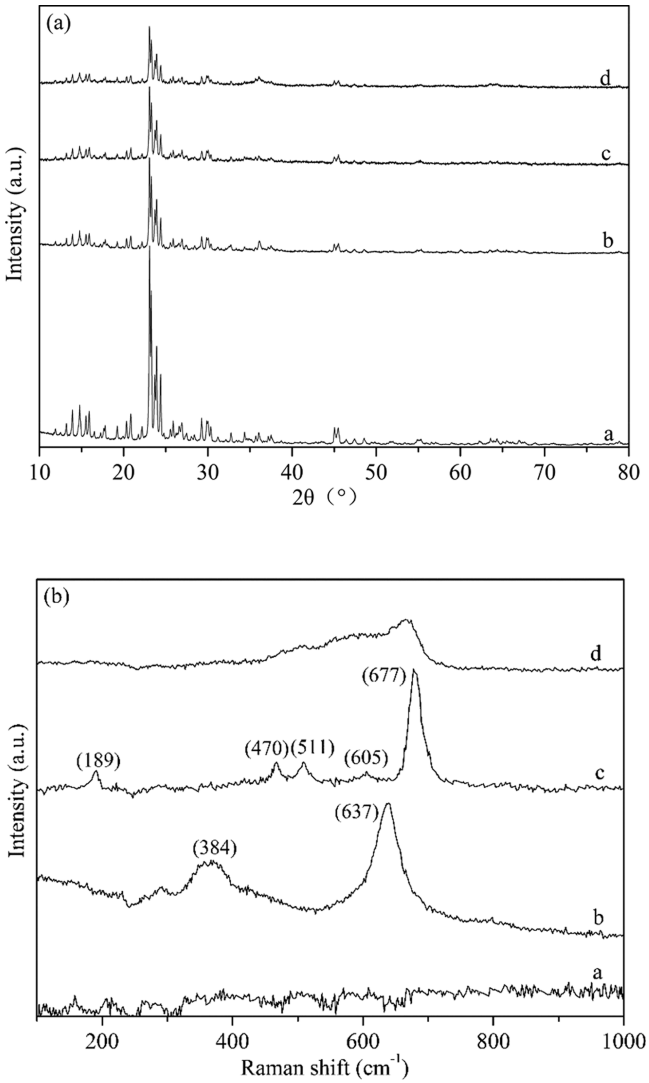

Figure 2. XRD (a) and Raman (b) patterns of the samples: a, HZSM-5; b, Mn/HZ-5; c, Co/HZ-5; d, MnCo/HZ-5.

Table 1. Characterization of the Fresh Catalysts

sample	atomic mass ratio[a] Mn	Co	A_{surface} (m^2 g^{-1})	D_{Pore} (nm)	V_{pore} (cm^3 g^{-1})	S_{particle}[b]
HZSM-5			2.06	0.21	2.06	48.02
Mn/HZ-5	9.85	0	4.22	0.27	4.22	49.41
Co/HZ-5	0	9.92	3.56	0.25	3.56	47.16
MnCo/HZ-5	9.88	9.96	4.72	0.30	4.72	43.19

[a]From ICPES. [b]Particle size, which was calculated based on the Scherrer equation.

Raman spectroscopy was performed to further study the crystallographic structure of the fresh catalysts. As presented in Figure 2b, no obvious band was found for the HZSM-5 catalysts. The characteristic bands for the Mn/HZ-5, Co/HZ-5, and MnCo/HZ-5 were in the range of 400−800 cm^{-1}. For the Mn/HZ-5 catalyst, the bands between 500−700 cm^{-1} were related to the stretching modes of MnO_6 octahedra, and the band at 384 cm^{-1} was related to the existence of α-MnO_2.[21] As for Co/HZ-5 catalyst, the bands centered at 470 (E_g), 677 (A_{1g}), 605 (F_{2g}), 511 (F_{2g}), and 189 (F_{2g}) cm^{-1} were the typical bands of spinel Co_3O_4.[12] The bands of MnCo/HZ-5 were broader and the peak intensities were lower in comparison with Mn/HZ-5 and Co/HZ-5, indicating the interaction of Co and Mn species,[22] which was in line with the result of XRD.

Table 1 presented the pore diameter, specific surface area, and total pore volume of the fresh catalysts. It is clearly shown that the HZSM-5 possesses the largest specific surface area (410.50 m^2 g^{-1}). Meanwhile, the MnCo/HZ-5 has the highest pore diameter (4.72 nm) and total pore volume (0.30 cm^3 g^{-1}). However, the average surface area decreased after the Mn and Co species loaded on the HZSM-5, and this was related to the blockage of pores by the presence of Mn and Co species.[13,19] In addition, the atomic mass ratios of Mn and Co of the different catalysts obtained by ICP analysis were reasonably close to the theoretical values within experimental and measurement error (Table 1).

3.1.2. Morphology and Elemental Analysis. The morphology and surface texture of the prepared catalysts were recorded by SEM, TEM, and HR-TEM. It could be found that the surface of HZSM-5 is very smooth, and some granules appeared after the Mn and Co loading on HZSM-5 as

DOI: 10.1021/acs.iecr.9b02668
Ind. Eng. Chem. Res. 2019, 58, 14719−14728

presented in Figure S1. As seen in HR-TEM images (Figure 3), the interplanar distances of 0.346 and 0.271 nm in the Mn/

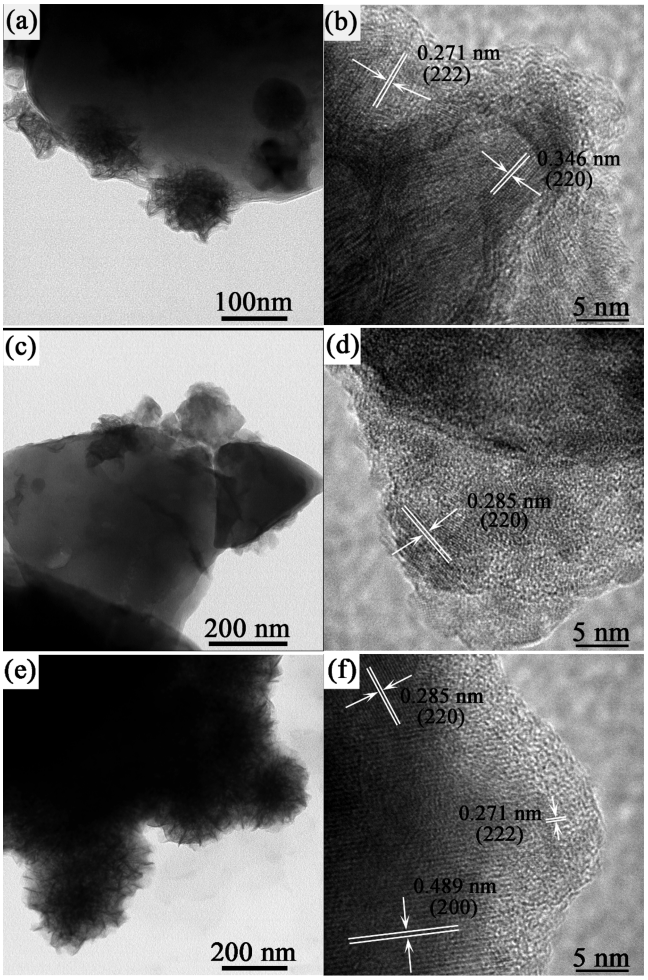

Figure 3. TEM and HRTEM patterns of Mn/HZ-5 (a,b), Co/HZ-5 (c,d), and MnCo/HZ-5 (e,f).

HZ-5 catalyst were attributed to the (220) plane of MnO_2 (JCPDS 44-141) and (222) facet of Mn_2O_3 (JCPDS 41-1442), respectively. The lattice fringes of the Co/HZ-5 catalyst with a spacing of 0.285 nm could be attributed to the (220) plane of Co_3O_4 (JCPDS 74-1657). The interplanar spacing of 0.489, 0.271, and 0.285 nm was observed in the MnCo/HZ-5 catalyst, which corresponds to the (200) plane of MnO_2, (222) plane of Mn_2O_3, and (220) plane of Co_3O_4, respectively. The EDX mapping of MnCo/HZ-5 catalysts (Figure S2) exhibits high and uniform dispersion of Mn and Co species.

The superficial elemental composition and their related oxidation state of the catalysts were analyzed via XPS. Figure S3 presented the survey spectra of all the fresh catalysts and used MnCo/HZ-5. As presented in Figure 4, the spectra of Mn 2p displayed two dominant peaks with binding energies of 642.3 and 653.8 eV, which were related to Mn $2p_{3/2}$ and Mn $2p_{1/2}$, respectively.[23] The Mn $2p_{3/2}$ spectrum was resolved into three peaks at 643.9, 641.1, and 642.4 eV, relating to Mn^{4+}, Mn^{2+}, and Mn^{3+}, respectively.[23,24] The calculation of the ratio of (Mn^{3+} + Mn^{4+})/Mn was obtained by the quantitative analysis of Mn $2p_{3/2}$ spectra. As presented in Table 2, the (Mn^{3+} + Mn^{4+})/Mn ratio of MnCo/HZ-5 is higher than that of Mn/HZ-5. The cobalt species were characterized by the Co

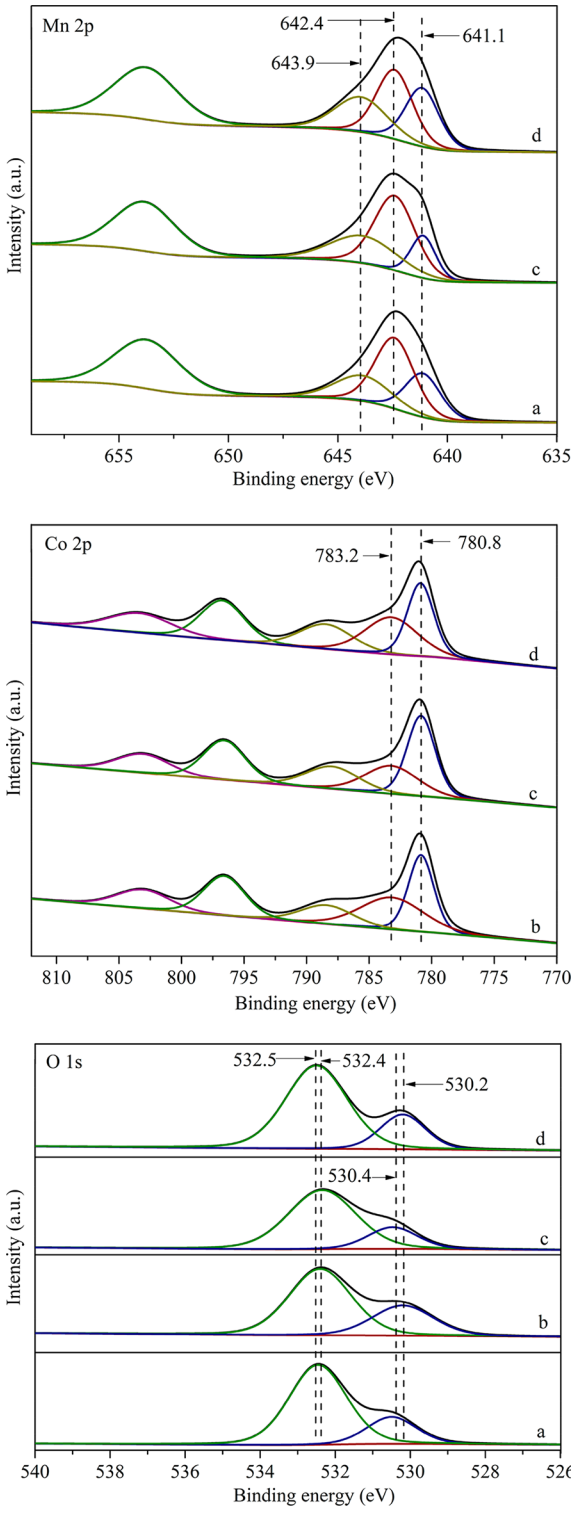

Figure 4. XPS patterns of Mn 2p, Co 2p, and O 1s (a, Mn/HZ-5; b, Co/HZ-5; c, MnCo/HZ-5; d, MnCo/HZ-5 used).

Table 2. Elemental Compositions of Mn−Co/HZSM-5 Catalysts

catalyst	Co^{2+}/Co^{3+}	Mn^{3+}/Mn	Mn^{4+}/Mn	O_a/O_l
Mn/HZ-5		0.48	0.24	3.4
Co/HZ-5	0.93			2.24
MnCo/HZ-5	1.07	0.51	0.31	3.70
MnCo/HZ-5 used	1.01	0.39	0.28	0.32

DOI: 10.1021/acs.iecr.9b02668
Ind. Eng. Chem. Res. 2019, 58, 14719−14728

$2p_{1/2}$ and Co $2p_{3/2}$ peaks located between 795 and 780.0 eV.[25] The XPS spectra of Co $2p_{3/2}$ was fitted with two peaks at 783.2 and 780.8 eV, which was corresponding to Co^{2+} and Co^{3+}, respectively.[26] Meanwhile, the small shoulder peak at 788.4 eV could be ascribed to the shake up satellite peak (Co^{2+}) of Co_3O_4.[26] Quantitatively, it was found that the MnCo/HZ-5 catalyst possesses the highest ratio of Co^{2+}/Co^{3+}. The O 1s XPS peaks of the as-prepared catalysts were split into two peaks located at 530.2 ± 0.2 eV and 532.3 ± 0.2 eV, corresponding to lattice oxygen species (O_l) and adsorbed oxygen species (O_a), respectively.[27] The ratio of O_a/O_l was calculated (shown in Table 2), and it decreased in the following order: MnCo/HZ-5 > Mn/HZ-5 > Co/HZ-5. It was generally recognized that the O_a possess higher activity than the O_l.[1] Additionally, they occupy a main role in the oxidation reactions because of their higher mobility.[1] Thus, higher content of O_a is conducive for the production of reactive oxygen species, which could further accelerate the oxidation of acetaldehyde.

3.1.3. H_2-TPR and NH_3-TPD Analysis. The reduction characteristics of the fresh catalysts were determined by H_2-TPR. As shown in Figure 5a, there was no distinct H_2 consumption peaks for the HZSM-5 support within the measured temperature range. For Mn/HZ-5, two obvious reduction peaks located around 343 and 460 °C were related to the reduction process of manganese from Mn^{4+} to Mn^{3+} and then to the reduction from Mn^{3+} to Mn^{2+}.[28] The Co/HZ-5 catalyst has a broad peak at 322 °C, which was in line with the reduction process of Co^{3+} to Co^{2+} and Co^{2+} to Co.[29,30] A higher temperature at 712 °C could be in association with the strong interaction between the support and Co species.[19,31] For MnCo/HZ-5 catalyst, the overlapped reduction peak at 266 °C was assigned to the reduction of $Mn^{4+} \rightarrow Mn^{3+}$ and $Co^{3+} \rightarrow Co^{2+}$, and the overlapped peak at 379 °C was attributed to the reduction of $Mn^{3+} \rightarrow Mn^{2+}$ and $Co^{2+} \rightarrow Co$. A higher reduction temperature at 656 °C was related to the strong interaction between Mn, Co species with support.[32,33] In addition, it can be concluded from the lower temperature shift and higher peak area of the reduction peak that the redox potential of MnCo/HZ-5 catalyst was higher than that of Co/HZ-5 and Mn/HZ-5. This could be related to the interaction between cobalt and manganese species in MnCo/HZ-5 catalyst.

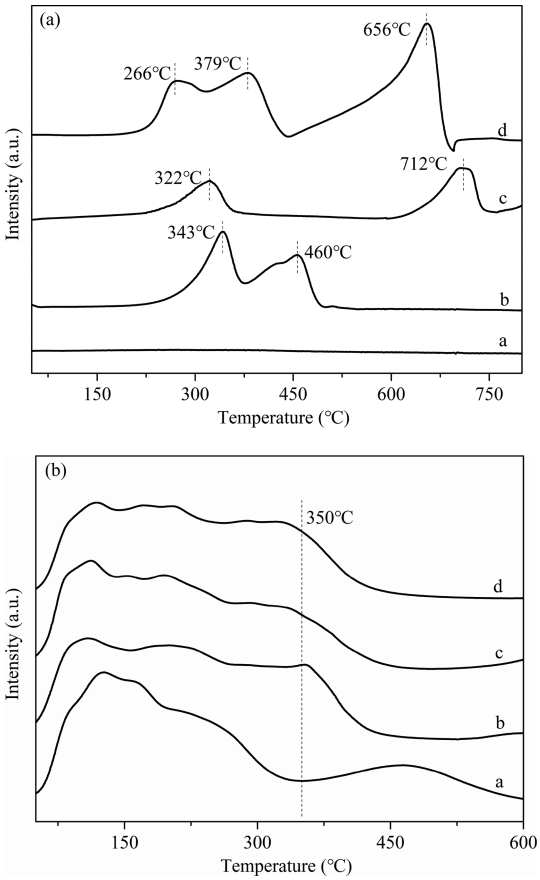

Figure 5. H_2-TPR (a) and NH_3-TPD (b) patterns of catalysts (a, HZSM-5; b, Mn/HZ-5; c, Co/HZ-5; d, MnCo/HZ-5)

As presented in Figure 5b, two desorption peaks were found in the NH_3-TPD curves at 50−350 °C and 350−600 °C. The former was ascribed to the successive desorption of NH_3 from Lewis acid sites, while the latter was ascribed to the desorption of NH_3 from Brönsted acid sites.[34] Accounting to the total peak area between 50 and 600 °C, the amount of the total acidity decreased in the following sequence: HZSM-5 > Mn/HZ-5 > MnCo/HZ-5 > Co/HZ-5. The loading of Mn and Co species on the HZSM-5 decreased the amount of acidity, which was in agreement with previous studies.[34,35] Moreover, this phenomenon also indicated that the acidity of these catalysts are not a determining factor for the catalytic activity because of the fact that the most active catalyst (MnCo/HZ-5) showed a lower acidity.

As presented in section 3.1, all the Mn−Co/HZ-5 catalysts showed no obvious changes in textural properties when compared to HZSM-5 support. The XPS results showed that the MnCo/HZ-5 catalyst possessed the highest (Mn^{3+} + Mn^{4+})/Mn, Co^{2+}/Co^{3+}, and O_a/O_l ratios. The redox pairs such as $Mn^{4+}-O^{2-}-Co^{2+}$ could promote the mobility and content of reactive oxygen species favor the oxidation of gas pollutants.[1] The H_2-TPR profiles showed that the MnCo/HZ-5 catalyst possessed the highest reducibility, indicating its easier activation and higher mobility of surface oxygen species.[2] All the above-mentioned properties of MnCo/HZ-5 catalysts are in close relation to its catalytic activity and consequently influenced the reaction performance.

3.2. Acetaldehyde Removal in the PPC System.

3.2.1. Effect of SED. Figure 6 presented the influence of SED on the $\eta_{acetaldehyde}$, EY, CO_2 yield, and CO_x yield in the NTP alone and PPC system. The gas flow rate was set as 1 L min^{-1}. It is obvious that increasing the SED promoted the $\eta_{acetaldehyde}$, CO_2 yield, and CO_x yield for all the cases. However, the EY varied inversely with the SED. Taking the NTP alone system for instance, increasing the SED from 80.25 to 380.03 J L^{-1}, the $\eta_{acetaldehyde}$, CO_2 yield, and CO_x yield took an increase from 32.41% to 77.14%, 8.70% to 23.70%, and 15.33% to 39.50%, respectively, while the EY yield decreased from 5.23 to 2.63 g kWh^{-1}. It is known that the higher energy favors the generation of high energy electrons and active species,[2] which are conducive for the formation of various oxidative species produced via collisions between carrier gas molecules and high-energy electrons, further accelerating the acetaldehyde oxidation process. It was reported that acetaldehyde dissociation in the NTP discharge region is divided into three pathways involving high-energy electrons, ions, and active radicals.[6] However, other report claimed that the reactions between VOCs and ions are negligible.[36] Klett et al.[37] also

DOI: 10.1021/acs.iecr.9b02668
Ind. Eng. Chem. Res. 2019, 58, 14719−14728

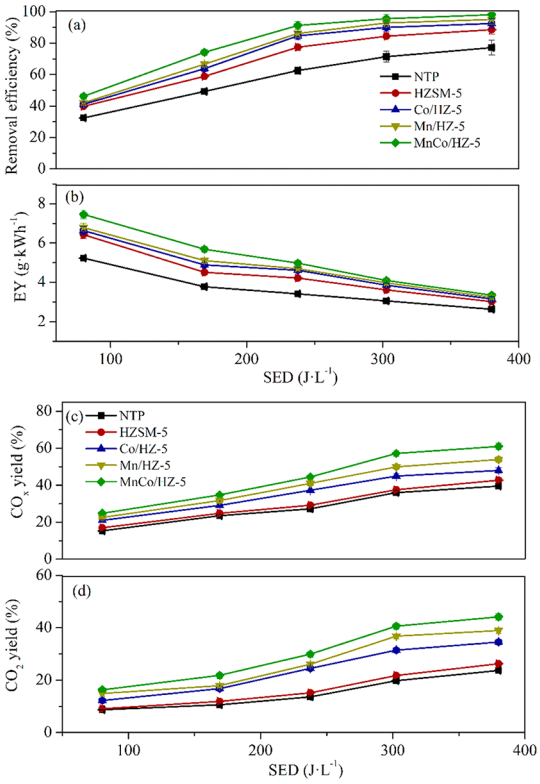

Figure 6. Effect of SED and catalysts on (a) the acetaldehyde removal efficiency, (b) EY, (c) CO_x yield, and (d) CO_2 yield.

reported that acetaldehyde destruction is controlled by two body reactions: high-energy electron impact and active radical (such as atomic oxygen, excited and metastable nitrogen species, hydroxyl radicals). Jia et al.[15] reported that reactions between acetaldehyde molecules and high-energy electrons and N_2* played a dominant role in the acetaldehyde destructions and the relative contribution of reactions between acetaldehyde and reactive species (N_2*, O, OH, and O_3) and high-energy electrons are dependent on the SED. The impact of the high-energy electrons on the carrier gas produces reactive species (such as O, $N_2(A)$, N_2*). The generation of these active species allows the stepwise decomposition and oxidation of acetaldehyde into CO_2, intermediates and other byproducts via the following equations: eqs 6−18.[15,37,38]

$$CH_3CHO + e \rightarrow CH_3 + CHO \quad (6)$$

$$CH_3CHO + N \rightarrow HCN + H_2 + CHO \quad (7)$$

$$CH_3CHO + N_2(A) \rightarrow CH_4 + CO + N_2(X) \quad (8)$$

$$CH_3CHO + N_2(A) \rightarrow CH_3 + CHO + N_2(X) \quad (9)$$

$$CH_3CHO + N_2^* \rightarrow CH_3CO + H + N_2(X) \quad (10)$$

$$CH_3CHO + N_2^* \rightarrow CH_3 + CHO + N_2(X) \quad (11)$$

$$CH_3CHO + O \rightarrow OH + CH_3CO \quad (12)$$

$$CH_3CHO + O \rightarrow CO + CH_3 + OH \quad (13)$$

$$CH_3CHO + OH \rightarrow H_2O + CH_3CO \quad (14)$$

$$CH_3CHO + OH \rightarrow H_2O + CH_2CHO \quad (15)$$

$$CH_3CO + (O/O_2) \rightarrow CO_2 + CH_3O \quad (16)$$

$$CH_3 + O \rightarrow CO + H + H_2 \quad (17)$$

$$CH_3CO + O_2 \rightarrow CO_2 + CH_3O_2 \quad (18)$$

3.2.2. Effect of Different Catalysts. As shown in Figure 6, in comparison with the NTP alone system, the $\eta_{acetaldehyde}$, EY yield, CO_2 yield, and CO_x yield were enhanced in the PPC system irrespective of the catalyst used. The presence of HZSM-5 catalyst markedly promoted the acetaldehyde removal efficiency. The large specific surface area of HZSM-5 provides many adsorption sites which prolong the detention time of the pollutant in the reaction zone, leading to higher EY and $\eta_{acetaldehyde}$. However, the CO_2 yield and CO_x yield were still too low, and it is essential to add active species to enhance the CO_2 and CO_x yield. The addition of Mn and Co oxides markedly improved the CO_x and CO_2 yield, with MnCo/HZ-5 exhibiting the highest catalytic activity. This increased catalytic performance of MnCo/HZ-5 was associated with the dispersion of Co and Mn species on the HZSM-5 support. As already presented in the H_2-TPR results, the MnCo/HZ-5 catalyst possesses a higher intensity of reduction peaks and lower reduction temperature. This manifested that MnCo/HZ-5 catalyst owned the highest mobility of surface oxygen species, promoting the acetaldehyde oxidation process. The XPS result also showed that MnCo/HZ-5 catalyst possess a higher quantity of adsorbed oxygen species, which could be conducive to the oxidation of acetaldehyde. Hence, more production of active surface oxygen species could boost the total oxidation of acetaldehyde.

After treated in the discharge region, the unreacted or partly reacted gas mixture was subsequently adsorbed onto the catalyst via surface active sites, which could further react with active surface oxygen to produce CO_2 and H_2O.[10] The interaction between cobalt and manganese species promotes the mobility of oxygen on the catalyst surface and enhances the conversion of lattice oxygen and oxygen molecules captured from the carrier gas to active oxygen species. In addition, ozone was dissociated to atomic oxygen by catalysts (as discussed below). Thus, active surface oxygen species had a crucial position in the catalytic reactions, which was generated from the lattice oxygen and ozone formed in the discharge region.[1]

3.2.3. Influence of Gas Flow Rate. The effect of gas flow rate on the acetaldehyde degradation in the NTP alone and PPC system is presented in Figure 7. As expected, the augment of gas flow rate decreased the CO_2 yield, CO_x yield and $\eta_{acetaldehyde}$. For example, in case of NTP combined with MnCo/HZ-5 catalyst, as the total gas flow rate increased from 0.5 L min^{-1} to 1.5 L min^{-1}, the CO_2 yield, CO_x yield, and $\eta_{acetaldehyde}$ decreased from 36.64% to 18.07%, 50.20% to 32.85%, and 99.27% to 75.24%, respectively. The retention time of acetaldehyde in the plasma discharge region was decreased due to the augment of the gas flow rate, which leads to insufficient reactions between the gaseous pollutants, reactive species, and high-energy electrons.[1,40] This results in decreased CO_2 yield, CO_x yield, and $\eta_{acetaldehyde}$. However, the augment of the gas flow rate led to a prominent improvement in the energy yield. The energy yield increased from 2.70 to 6.15 g kWh^{-1} when the gas flow rate raised from 0.5 to 1.5 L min^{-1}.

3.3. O_3 Formation. The concentration of O_3 generated in the NTP alone and PPC system was shown in Figure 8. In all the cases, the amount of O_3 produced increased with the

DOI: 10.1021/acs.iecr.9b02668
Ind. Eng. Chem. Res. 2019, 58, 14719−14728

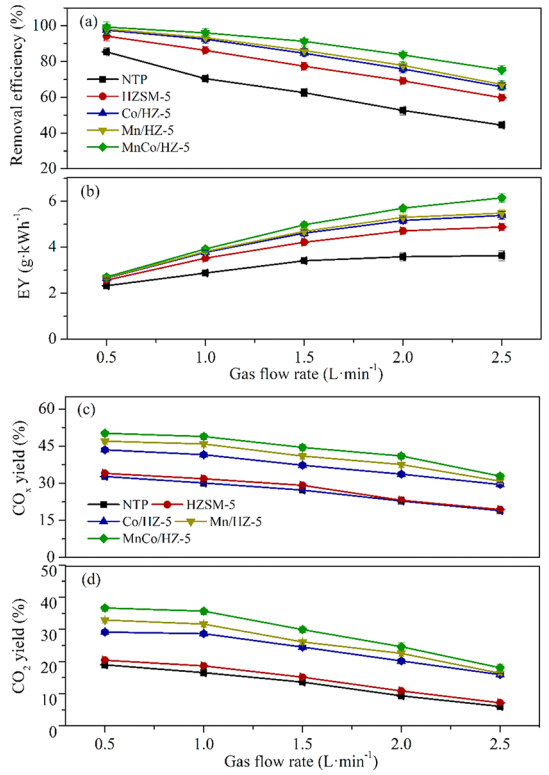

Figure 7. Influence of gas flow rate on (a) the acetaldehyde removal efficiency, (b) EY, (c) CO_x yield, and (d) CO_2 yield.

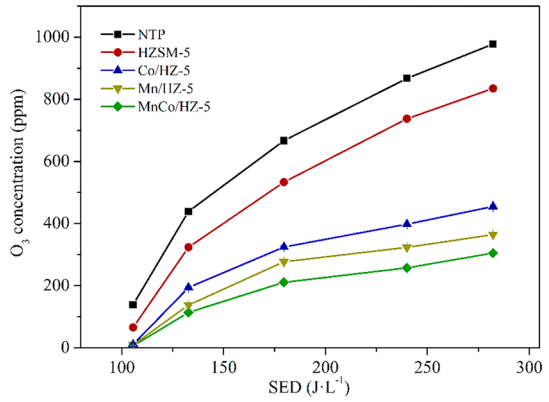

Figure 8. Influence of different catalysts on the production of O_3 in the NTP and PPC systems.

increase of SED. The PPC system packed with Mn−CoO_x/HZ produced less O_3 in comparison with the NTP system. For instance, the concentration of O_3 at the SED of 200.1 J L^{-1} in NTP system and PPC system with MnCo/HZ-5 was 733.60 and 226.33 ppm, respectively. The generation of O_3 was via the collisions between high-energy electrons and oxygen in the discharge region according to eqs 19−21.[3,6] The O_3 thus formed was decomposed to form active atomic oxygen by the catalyst as shown in eqs 23 and 24 (* donated as surface active sites of the catalyst),[6] which participates in the pollutant oxidation reactions.

$$e^- + O_2 \rightarrow O^- + O \quad (19)$$

$$e^- + O_2 \rightarrow O + O + e^- \quad (20)$$

$$O + O_2 \rightarrow O_3 \quad (21)$$

$$O_3 + * \rightarrow O^* + O_2 \quad (22)$$

$$O_3 + O^* \rightarrow O_2^* + O_2 \quad (23)$$

$$O_2^* \rightarrow O_2 + * \quad (24)$$

3.4. Reaction Kinetics. In the PPC system, acetaldehyde molecules were first destructed by high-energy electrons, ion collisions, and reactive radicals like $OH^\bullet$ and $O^\bullet$ and then oxidized by surface active oxygen species.[10,39] The rate coefficient of each elementary reaction included in the NTP-catalytic degradation process of VOCs is difficult to determine as a result of that the concentrations of radicals and intermediate species during the destruction were difficult to detect. Moreover, no comprehensive model has been established to describe the interactions between NTP and catalysts for the reactions in the whole NTP-catalytic degradation process for VOC elimination. Thus, we selected a simple model to describe the PPC system, assuming a plug flow.[40,41]

The rate of acetaldehyde degradation (γ_{CH3CHO}) could be expressed as

$$-\frac{dc}{dt} = (k_e \times C_e + k_{ion}C_{ion} + k_N C_N + k_O C_O + k_{O_3}C_{O_3} + k_H C_H + k_{OH}C_{OH}) \times C_{CH_3CHO} \quad (25)$$

where C_e, C_{ion}, C_N, C_O, C_{O3}, C_H, C_{OH}, and C_{CH3CHO} represent the concentration of high-energy electrons, ions, N-containing species, $O^\bullet$, $H^\bullet$, O_3, $OH^\bullet$, and acetaldehyde, and k_e, k_{ion}, k_N, k_O, k_{O3}, k_H, and k_{OH} represent their respective reaction rate constants.

Table 3 showed the reaction constants of the main reactions in the acetaldehyde degradation process. The effect of O_3 on

Table 3. Main Reactions Cited in the Paper

reaction	K_{300} (cm^3 mol^{-1} s^{-1})	ref
$CH_3CHO + e^- \rightarrow$ products + e^-		4
$CH_3CHO + N \rightarrow HCN + H_2 + CHO$	2×10^{-14}	43
$CH_3CHO + N_2$ (A) $\rightarrow CH_3$+ CHO + N_2 (X)	1×10^{-10}	37
$CH\ CHO + N_2^* \rightarrow CH_3 + CHO + N_2$(X)	5×10^{-10}	37
$CH_3CHO + O \rightarrow OH + CH_3CO$	4.6×10^{-13}	37
$CH_3CHO+O_3 \rightarrow$ products	3.4×10^{-20}	44
$CH_3CHO + H \rightarrow H_2 + CH_3CO$	7.95×10^{-14}	45
$CH_3CHO + OH \rightarrow H_2O + CH_3CO$	1.5×10^{-11}	37

acetaldehyde elimination was ignored, owing to its small reaction constant. The rate constants of the reaction between N, H, and acetaldehyde were lower than that of N_2 metastable states. Thus, the effect of N and H radicals on acetaldehyde abatement was ignored. The rate constant of the reaction between O species and acetaldehyde were lower than that of N_2 metastable states, but the concentration of O is higher than N_2 metastable states as reported in the previous report.[42] Meanwhile, the effect of OH was also neglected due to its low density.[42] The electron collisions were neglected due to their short lifetime and low density. In the view of that the concentrations of N_2 metastable states and O species are constant under fixed air pressure and electric field,[42] eq 25 could be simplified as

$$-\frac{dc}{dt} = k \times C_{acetaldehyde} \quad (26)$$

DOI: 10.1021/acs.iecr.9b02668
Ind. Eng. Chem. Res. 2019, 58, 14719−14728

where k is donated as the apparent rate constant.

Integrating eq 26 resulted in the following:

$$-\ln \frac{C_{out}}{C_{in}} = kt \tag{27}$$

In view of eq 1, eq 27 could be expressed as follows:

$$-\ln(1 - \eta_{acetaldehyde}) = kt \tag{28}$$

Figure 9 showed the relationship between the $-\ln(1 - \eta_{acetaldehyde})$ and time for different catalysts. The slope of the line gives the apparent rate constant. As shown in Table 4, all the regression coefficients (R^2) were greater than 0.99, indicating that the linear fitting was statistically acceptable. Compared to the NTP alone system, the introduction of catalysts increased the rate constant, with the MnCo/HZ-5 catalyst exhibiting the highest rate constant. This was in agreement with the highest acetaldehyde removal efficiency obtained by the combination of NTP and MnCo/HZ-5 catalyst. This phenomenon indicated that the combination of NTP with the catalysts enhanced acetaldehyde oxidation.

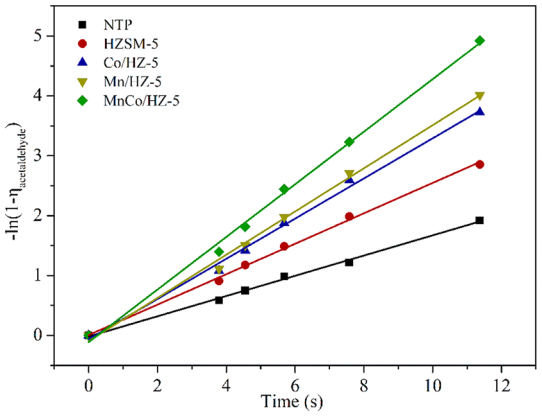

Figure 9. Rate constants of acetaldehyde removal in the NTP and PPC systems.

Table 4. Apparent Rate Constants and Regression Coefficients in the NTP and PPC Systems

	NTP	HZSM-5	Mn/HZ-5	Co/HZ-5	MnCo/HZ-5
k	0.17	0.25	0.34	0.36	0.44
R^2	0.9967	0.9974	0.9943	0.9945	0.9958

4. CONCLUSIONS

The Mn−Co/HZSM-5 catalysts synthesized via the deposition−precipitation method were applied in the PPC system for acetaldehyde removal. The combination of the catalyst with NTP showed a notable advance in the acetaldehyde removal efficiency, CO_2 yield, CO_x yield, and EY and greatly inhibited the formation of O_3. The mixed MnCo/HZSM-5 showed the best activity in the PPC system for acetaldehyde removal, which was related to the crystal structure, redox property, and surface adsorbed oxygen species. Additionally, the acetaldehyde removal efficiency, CO_2 yield, and CO_x yield increased with increasing the SED but decreased with increasing the gas flow rate. However, the EY was reduced with the increase of SED and promoted with the augment of the gas flow rate. Moreover, the reaction kinetics results showed that the acetaldehyde removal in the PPC system was a typical first-order reaction. The addition of catalysts markedly promoted the acetaldehyde degradation process, with the mixed MnCo/HZ-5 exhibiting the highest apparent rate constant.

■ ASSOCIATED CONTENT

Supporting Information

The Supporting Information is available free of charge on the ACS Publications website at DOI: 10.1021/acs.iecr.9b02668.

Figures containing SEM images for the morphologies of the prepared catalysts, EDX mapping for the dispersion analysis of elements (Si, Al, Mn, Co, and O) of MnCo/HZ-5 catalyst, and XPS survey of the prepared catalysts (PDF)

■ AUTHOR INFORMATION

Corresponding Author

*E-mail: zxshen@mail.xjtu.edu.cn.

ORCID

Tian Chang: 0000-0001-7339-3624

Zhenxing Shen: 0000-0002-1294-1751

Yu Huang: 0000-0003-3334-4849

Savita K. P. Veerapandian: 0000-0003-4652-8487

Notes

The authors declare no competing financial interest.

■ ACKNOWLEDGMENTS

This research was supported by the project "DepollutAir" of Interreg V France-Wallonie-Vlaanderen, the National Science Foundation of China (NSFC, Grant 41573138), State Key Laboratory of Loess and Quaternary Geology, Institute of Earth Environment, CAS (Grant SKLLQG1616), and China Scholarship Council (CSC, Grant No. 201806280087). Yu Huang is also supported by the "Hundred Talent Program" of the Chinese Academy of Sciences.

■ ABBREVIATIONS

$A_{surface}$ = specific surface area
C_{CH3CHO} = concentration of acetaldehyde
C_e = concentration of high-energy electrons
C_H = concentration of hydrogen
C_{ion} = concentration of ions
C_N = concentration of nitrogen-containing species
C_O = concentration of active oxygen
CO_2 = carbon dioxide
C_{O3} = concentration of ozone
CO = carbon monoxide
C_{OH} = concentration of hydroxide radical
CO_x = carbon monoxide + carbon dioxide
D_{Pore} = average pore diameter
DBD = dielectric barrier discharge
EDX = energy dispersive X-ray
eq = equation
EY = energy yied
FTIR = Fourier transform infrared spectroscopy
GC = gas chromatography
H_2-TPR = hydrogen temperature-programmed reduction
HZ-5 = HZSM-5
H_2O = water

DOI: 10.1021/acs.iecr.9b02668
Ind. Eng. Chem. Res. 2019, 58, 14719−14728

HR-TEM = high-resolution-transmission electron microscopy
ICPES = inductively coupled plasma emission spectrometry
k_e = reaction rate constant of high-energy electrons
k_H = reaction rate constant of hydrogen
k_{ion} = reaction rate constant of ions
k_N = reaction rate constant of nitrogen-containing species
k_O = reaction rate constant of active oxygen
k_{O3} = reaction rate constant of ozone
k_{OH} = reaction rate constant of hydroxide radical
$M_{acetaldehyde}$ = molar mass of acetaldehyde
MFC = mass flow controller
NH_3-TPD = ammonia-temperature programmed desorption
NTP = nonthermal plasma
N_2 = nitrogen
O_3 = ozone
O_2 = oxygen
ppm = parts per million
$S_{particle}$ = average pore diameter
SED = specific energy density
SEM = scanning electron microscopy
VOCs = volatile organic compound
V_m = molar volume
V_{pore} = total pore volume
XPS = X-ray photoelectron spectroscopy
XRD = X-ray diffraction
$\eta_{acetaldehyde}$ = acetaldehyde removal efficiency

REFERENCES

(1) Wang, B. W.; Chi, C. M.; Xu, M.; Wang, C.; Meng, D. J. Plasma-catalytic removal of toluene over CeO_2-MnO_x catalysts in an atmosphere dielectric barrier discharge. *Chem. Eng. J.* **2017**, *322*, 679.
(2) Zhu, X. B.; Tu, X.; Mei, D. H.; Zheng, C. H.; Zhou, J. S.; Gao, X.; Luo, Z. Y.; Ni, M. J.; Cen, K. F. Investigation of hybrid plasma-catalytic removal of acetone over CuO/gamma-Al_2O_3 catalysts using response surface method. *Chemosphere* **2016**, *155*, 9.
(3) Guo, Y. F.; Ye, D. Q.; Chen, K. F.; He, J. C.; Chen, W. L. Toluene decomposition using a wire-plate dielectric barrier discharge reactor with manganese oxide catalyst in situ. *J. Mol. Catal. A: Chem.* **2006**, *245*, 93.
(4) Koeta, O.; Blin-Simiand, N.; Faider, W.; Pasquiers, S.; Bary, A.; Jorand, F. Decomposition of Acetaldehyde in Atmospheric Pressure Filamentary Nitrogen Plasma. *Plasma Chem. Plasma Process.* **2012**, *32*, 991.
(5) Jiang, N.; Lu, N.; Li, J.; Wu, Y. Degradation of Benzene by Using a Silent-Packed Bed Hybrid Discharge Plasma Reactor. *Plasma Sci. Technol.* **2012**, *14*, 140.
(6) Huang, H. B.; Ye, D. Q.; Leung, D. Y. C.; Feng, F. D.; Guan, X. J. Byproducts and pathways of toluene destruction via plasma-catalysis. *J. Mol. Catal. A: Chem.* **2011**, *336*, 87.
(7) Chen, H. L.; Lee, H. M.; Chen, S. H.; Chang, M. B.; Yu, S. J.; Li, S. N. Removal of Volatile Organic Compounds by Single-Stage and Two-Stage Plasma Catalysis Systems: A Review of the Performance Enhancement Mechanisms, Current Status, and Suitable Applications. *Environ. Sci. Technol.* **2009**, *43*, 2216.
(8) Cui, S. P.; Hao, R. L.; Fu, D. An integrated system of dielectric barrier discharge combined with wet electrostatic precipitator for simultaneous removal of NO and SO_2: Key factors assessments, products analysis and mechanism. *Fuel* **2018**, *221*, 12.
(9) Cui, S. P.; Hao, R. L.; Fu, D. Integrated method of non-thermal plasma combined with catalytical oxidation for simultaneous removal of SO2 and NO. *Fuel* **2019**, *246*, 365.
(10) Li, Y. Z.; Fan, Z. Y.; Shi, J. W.; Liu, Z. Y.; Zhou, J. W.; Shangguan, W. F. Modified manganese oxide octahedral molecular sieves M′-OMS-2 (M′=Co, Ce, Cu) as catalysts in post plasma-catalysis for acetaldehyde degradation. *Catal. Today* **2015**, *256*, 178.
(11) Ma, J. Z.; Wang, C. X.; He, H. Transition metal doped cryptomelane-type manganese oxide catalysts for ozone decomposition. *Appl. Catal., B* **2017**, *201*, 503.
(12) Zheng, Y. L.; Wang, W. Z.; Jiang, D.; Zhang, L. Amorphous MnO_x modified Co_3O_4 for formaldehyde oxidation: improved low-temperature catalytic and photothermocatalytic activity. *Chem. Eng. J.* **2016**, *284*, 21.
(13) Zhang, C. H.; Huang, H.; Li, G. Q.; Wang, L.; Song, L.; Li, X. B. Zeolitic acidity as a promoter for the catalytic oxidation of toluene over MnO_x /HZSM-5 catalysts. *Catal. Today* **2019**, *327*, 374.
(14) Veerapandian, S. K. P.; De Geyter, N.; Giraudon, J.-M.; Lamonier, J.-F.; Morent, R. The Use of Zeolites for VOCs Abatement by Combining Non-Thermal Plasma, Adsorption, and/or Catalysis: A Review. *Catalysts* **2019**, *9*, 98.
(15) Jia, Z. X.; Vega-Gonzalez, A.; Amar, M. B.; Hassouni, K.; Tieng, S.; Touchard, S.; Kanaev, A.; Duten, X. Acetaldehyde removal using a diphasic process coupling a silver-based nano-structured catalyst and a plasma at atmospheric pressure. *Catal. Today* **2013**, *208*, 82.
(16) Chang, T.; Shen, Z. X.; Huang, Y.; Lu, J. Q.; Ren, D. X.; Sun, J.; Cao, J. J.; Liu, H. X. Post-plasma-catalytic removal of toluene using MnO_2−Co_3O_4 catalysts and their synergistic mechanism. *Chem. Eng. J.* **2018**, *348*, 15.
(17) Chang, T.; Lu, J. Q.; Shen, Z. X.; Huang, Y.; Lu, D.; Wang, X.; Cao, J. J.; Morent, R. Simulation and optimization of the post plasma-catalytic system for toluene degradation by a hybrid ANN and NSGA-II method. *Appl. Catal., B* **2019**, *244*, 107.
(18) Wang, T.; Wan, Z. T.; Yang, X. C.; Zhang, X. Y.; Niu, X. X.; Sun, B. M. Promotional effect of iron modification on the catalytic properties of Mn-Fe/ZSM-5 catalysts in the Fast SCR reaction. *Fuel Process. Technol.* **2018**, *169*, 112.
(19) Cao, X. X.; Zhou, R.; Rui, N.; Wang, Z. Y.; Wang, J. J.; Zhou, X. T.; Liu, C. J. Co_3O_4/HZSM-5 catalysts for methane combustion: The effect of preparation methodologies. *Catal. Today* **2017**, *297*, 219.
(20) Tu, X.; Gallon, H. J.; Whitehead, J. C. Plasma-assisted reduction of a NiO/Al_2O_3 catalyst in atmospheric pressure H_2/Ar dielectric barrier discharge. *Catal. Today* **2013**, *211*, 120.
(21) Gao, T.; Fjellvåg, H.; Norby, P. A comparison study on Raman scattering properties of α- and β-MnO_2. *Anal. Chim. Acta* **2009**, *648*, 235.
(22) Tian, Z.-Y.; Tchoua Ngamou, P. H.; Vannier, V.; Kohse-Hoinghaus, K.; Bahlawane, N. Catalytic oxidation of VOCs over mixed Co−Mn oxides. *Appl. Catal., B* **2012**, *117*−*118*, 125.
(23) Yan, Y.; Wang, L.; Zhang, H. P.; Zhang, X. Y. Catalytic combustion of isopropanol over Co-Mn mixed oxides modified ZSM-5 zeolite membrane catalysts coated on stainless steel fibers. *Sep. Purif. Technol.* **2017**, *175*, 213.
(24) Du, X. Y.; Li, C. T.; Zhao, L. K.; Zhang, J.; Gao, L.; Sheng, J. J.; Yi, Y. Y.; Chen, J. Q.; Zeng, G. M. Promotional removal of HCHO from simulated flue gas over Mn-Fe oxisdes modified activated coke. *Appl. Catal., B* **2018**, *232*, 37.
(25) Zhu, Z. Z.; Lu, G. Z.; Zhang, Z. G.; Guo, Y.; Guo, Y. L.; Wang, Y. Q. Highly Active and Stable Co_3O_4/ZSM-5 Catalyst for Propane Oxidation: Effect of the Preparation Method. *ACS Catal.* **2013**, *3*, 1154.
(26) Xie, X. H.; Deng, J. G.; Zang, S. M.; Yang, H. G.; Guo, G. S.; Arandiyan, H.; Dai, H. X. Au−Pd/3DOM Co_3O_4: Highly active and stable nanocatalysts for toluene oxidation. *J. Catal.* **2015**, *322*, 38.
(27) Cai, Y.; Zhu, X.; Hu, W.; Zheng, C.; Yang, Y.; Chen, M.; Gao, X. Plasma-catalytic decomposition of ethyl acetate over $LaMO_3$ (M = Mn, Fe, and Co) perovskite catalysts. *J. Ind. Eng. Chem.* **2019**, *70*, 447.
(28) Weng, X. L.; Sun, P. F.; Long, Y.; Meng, Q. J.; Wu, Z. B. Catalytic Oxidation of Chlorobenzene over $Mn_xCe_{1-x}O_2$/HZSM-5 Catalysts: A Study with Practical Implications. *Environ. Sci. Technol.* **2017**, *51*, 8057.
(29) Li, H. H.; Wang, Y.; Wang, S. K.; Wang, X.; Hu, J. J. Promotional effect of Mo addition on CoO_x/Ti-Ce catalyst for oxidation removal of elemental mercury in flue gas. *Fuel* **2018**, *224*, 424.

DOI: 10.1021/acs.iecr.9b02668
Ind. Eng. Chem. Res. 2019, 58, 14719−14728

(30) Ren, X. Y.; Cao, J. P.; Zhao, X. Y.; Shen, W. Z.; Wei, X. Y. Increasing light aromatic products during upgrading of lignite pyrolysis vapor over Co-modified HZSM-5. *J. Anal. Appl. Pyrolysis* **2018**, *130*, 190.
(31) Ferencz, Z.; Varga, E.; Puskás, R.; Kónya, Z.; Baán, K.; Oszkó, A.; Erdőhelyi, A. Reforming of ethanol on Co/Al_2O_3 catalysts reduced at different temperatures. *J. Catal.* **2018**, *358*, 118.
(32) Kovanda, F.; Jirátová, K.; Ludvíková, J.; Raabová, H. Co-Mn-Al mixed oxides on anodized aluminum supports and their use as catalysts in the total oxidation of ethanol. *Appl. Catal., A* **2013**, *464−465*, 181.
(33) Jirátová, K.; Mikulová, J.; Klempa, J.; Grygar, T.; Bastl, Z.; Kovanda, F. Modification of Co-Mn-Al mixed oxide with potassium and its effect on deep oxidation of VOC. *Appl. Catal., A* **2009**, *361*, 106.
(34) Cheng, S. Y.; Wei, L.; Julson, J.; Muthukumarappan, K.; Kharel, P. R. Upgrading pyrolysis bio-oil to biofuel over bifunctional Co-Zn/HZSM-5 catalyst in supercritical methanol. *Energy Convers. Manage.* **2017**, *147*, 19.
(35) Tshabalala, T. E.; Coville, N. J.; Scurrell, M. S. Methane dehydroaromatization over modified Mn/H-ZSM-5 zeolite catalysts: Effect of tungsten as a secondary metal. *Catal. Commun.* **2016**, *78*, 37.
(36) Lee, H. M.; Chang, M. B. Abatement of Gas-phase p-Xylene via Dielectric Barrier Discharges. *Plasma Chem. Plasma Process.* **2003**, *23*, 541.
(37) Klett, C.; Touchard, S.; Vegagonzalez, A.; Redolfi, M.; Bonnin, X.; Hassouni, K.; Duten, X. Experimental and modeling study of the oxidation of acetaldehyde in an atmospheric-pressure pulsed corona discharge. *Plasma Sources Sci. Technol.* **2012**, *21*, 045001.
(38) Lee, H. M.; Chang, M. B. Gas-Phase Removal of Acetaldehyde via Packed-Bed Dielectric Barrier Discharge Reactor. *Plasma Chem. Plasma Process.* **2001**, *21*, 329.
(39) Wang, W. Z.; Wang, H. L.; Zhu, T. L.; Fan, X. Removal of gas phase low-concentration toluene over Mn, Ag and Ce modified HZSM-5 catalysts by periodical operation of adsorption and non-thermal plasma regeneration. *J. Hazard. Mater.* **2015**, *292*, 70.
(40) Kim, K.; Johnston, K. P. Molecular Interactions in Dilute Supercritical Fluid Solutions. *Ind. Eng. Chem. Res.* **1987**, *26*, 1206.
(41) Bird, R. B.; Stewart, W. E.; Lightfoot, E. N. *Transport Phenomena*; Wiley: New York, 1960.
(42) Huang, H. B.; Ye, D. Q.; Leung, D. Y. C. Abatement of Toluene in the Plasma-Driven Catalysis: Mechanism and Reaction Kinetics. IEEE T. *IEEE Trans. Plasma Sci.* **2011**, *39*, 877.
(43) Lambert, R. M.; Christie, M. I.; Golesworthy, R. C.; Linnett, J. W. Mass Spectrometric Study of the Reaction of Nitrogen Atoms with Acetaldehyde. *P. R. Soc. London* **1968**, *302*, 167.
(44) Stedman, D. H.; Niki, H. Ozonolysis rates of some atmospheric gases. *Environ. Lett.* **1973**, *4*, 303.
(45) Baulch, D. L.; Cobos, C. J.; Cox, R. A.; Frank, P.; Hayman, G.; Just, T.; Kerr, J. A.; Murrells, T.; Pilling, M. J.; Troe, J.; Walker, R. W.; Warnatz, J. Summary table of evaluated kinetic data for combustion modeling: Supplement 1. *Combust. Flame* **1994**, *98*, 59.

DOI: 10.1021/acs.iecr.9b02668
Ind. Eng. Chem. Res. 2019, 58, 14719−14728